Hybrid membranes of lipids and diblock copolymers: From homogeneity to rafts to phase separation

Ssu-Wei Hu,[1] Chun-Yen Huang,[2] Heng-Kwong Tsao,[1,3,*] and Yu-Jane Sheng[2,†]

[1]*Department of Chemical and Materials Engineering, National Central University, Jhongli, Taiwan 320, Republic of China*

[2]*Department of Chemical Engineering, National Taiwan University, Taipei, Taiwan 106, Republic of China*

[3]*Department of Physics, National Central University, Jhongli, Taiwan 320, Republic of China*

(Received 29 June 2018; published 3 January 2019)

Hybrid lipid-polymer vesicles can integrate benefits of liposomes and polymersomes. In this work, the phase behavior of hybrid membranes containing lipids and diblock copolymers is explored by dissipative particle dynamics simulations. The influences of lipid unsaturation and thickness mismatch between lipids and polymers are considered. The transition from the mixing state (homogeneous distribution) to the demixing state (formation of bilayered lipid-rich domains) is always observed as the lipid concentration (φ_l) exceeds a critical value, which increases with the degree of unsaturation. It is found that phase separation is driven by weak energy incompatibility between the hydrophobic segments of lipids and polymers. When the effect of thickness mismatch becomes significant, the occurrence of the demixing state is retarded, and monolayer lipid rafts emerge before phase separation. Lipid fluidity associated with the physical state of a hybrid membrane can be characterized by lateral lipid diffusivity (D_l). In the polymer-rich membrane, D_l is higher in the mixing state, but decreases generally with φ_l due to lipid-lipid interactions and interdigitation.

DOI: 10.1103/PhysRevE.99.012403

I. INTRODUCTION

Lipids and diblock copolymers are natural and synthetic amphiphiles which possess both hydrophilic and hydrophobic moieties. They can self-assemble into a rich variety of order structures, such as micelles [1,2] and bilayer membranes [3,4], in a selective solvent. Upon certain conditions, both lipid and polymeric bilayer membranes can further curl to form lipid vesicles (liposomes) and polymeric vesicles (polymersomes), respectively. Liposomes have been used in the field of biological technologies such as encapsulation of biomolecules [5–7] and targeted drug delivery [8–10] because they are nontoxic, biodegradable, and easily functionalized with proteins or ligands. However, low mechanical stability and high leakiness of liposomes restrain their applications mainly because of their small membrane thickness [11]. In contrast to liposomes, artificial polymersomes exhibit superior properties in terms of long-term stability and mechanical strength. Furthermore, the use of synthetic polymers makes membrane characteristics tunable and thus the properties of polymersomes such as permeability can be controlled [12–15]. Although polymersomes have many attractive properties, poor biocompatibility and biofunctionality as compared to natural liposomes increase potential health risk, especially when used for *in vivo* applications. In order to incorporate the biocompatibility of liposomes with the robustness and chemical versatility of polymersomes, hybrid vesicles containing both phospholipids and block copolymers have been highlighted in recent years [16–20].

The properties of hybrid membranes are usually explored through the study of giant unilamellar vesicles (GUVs) prepared by electroformation [11,18]. It has been reported that the stability and morphological characteristics of hybrid membranes are governed by the molar composition of the lipid and polymer and the physical state of the lipids [16–18,21]. For lipid-rich membranes, the vesicular structures were apt to undergo a budding process [11]. In contrast, in polymer-rich membranes, the hybrid vesicles generally display higher stability. At the same molar composition, the morphological features of the membrane will change if the physical state (fluidity) of the lipids is altered. It is well known that the physical state of lipids is mainly dependent on their main chain transition temperature (T_m), at which the lipid bilayer undergoes a transition from ordered gel phase to liquid phase. At low system temperature $T < T_m$, lipids exist in the gel phase, and they are laterally ordered (less fluidity) in the lipid membrane. At high temperature $T > T_m$, lipids are in the liquid phase, and they can move around more (higher fluidity) in the membrane. Experimental results have shown that lipid fluidity is able to trigger the mixing-demixing transition of lipids in a polymer-rich membrane [11,16]. A homogeneous distribution of lipids (mixing) in the hybrid membrane appears as the lipid is in the liquid state. On the contrary, the formation of lipid-rich domains (demixing) is observed as the lipid is in its gel phase. That is, both polymer-rich and lipid-rich domains coexist, corresponding to phase separation.

In addition to composition and fluidity, the energy incompatibility of hydrophobic segments between lipids and copolymers also plays an important role on the phase behavior of hybrid membranes [11,16,18]. The energy incompatibility between two species is often estimated by the difference of their solubility parameters ($\Delta\delta$). The incompatibility rises

*hktsao@cc.ncu.edu.tw
†yjsheng@ntu.edu.tw

as $\Delta\delta$ increases. In general, $\Delta\delta$ between the fatty acid tail (FAT) in phospholipids and the hydrophobic moieties in copolymers is small. For example, poly(butadiene) (PB) and poly(isobutylene) (PIB) are two common hydrophobic moieties in copolymers used for the formation of hybrid membranes. One has $\Delta\delta \approx 0.8$ cal$^{1/2}$/cm$^{3/2}$ for FAT-PB, and $\Delta\delta \approx 1.4$ cal$^{1/2}$/cm$^{3/2}$ for FAT-PIB [22–24]. Note that $\Delta\delta \approx 32$ cal$^{1/2}$/cm$^{3/2}$ for water and n-dodecane. Owing to their small values of $\Delta\delta$, the energy incompatibility between lipids and copolymers is insignificant. This weak incompatibility has been proposed as a basic requirement to enable the formation of hybrid membranes. Nevertheless, the emergence of phase separation of lipid and polymer implies that the energy incompatibility is still strong enough. On the basis of the above argument, the increment of the hydrophobic length of the copolymers, which enhances the incompatibility, should benefit the domain formation of the lipid and polymer in the hybrid membrane. However, previous studies have demonstrated that a single-phase membrane (mixing state) was favorable as the hydrophobic length of copolymers is long enough [16,18,19]. This phenomenon indicates that the thickness mismatch caused by the increment of the hydrophobic length of copolymers is another crucial factor for phase separation in the hybrid membranes.

Although there have been a few experimental efforts to investigate the properties and morphologies of hybrid membranes [11,16–20], their microscopic molecular structures are not unveiled directly due to the limitation of detection methodologies. In addition, the parameters governing the phase behavior of hybrid lipid-polymer vesicles and the corresponding mechanisms are also unclear. Further studies via molecular simulations are useful for providing both a better understanding and a certain predictability. In this work, a hybrid tensionless membrane assembled by lipids and diblock copolymers is explored by dissipative particle dynamics (DPD) in an ensemble of constant number, pressure, surface tension, and temperature ($NP\gamma T$) [25,26]. The influences of the molar composition, lipid fluidity, incompatibility between moieties, and thickness mismatch on the phase behavior of hybrid membranes are studied systematically.

II. MODEL AND SIMULATION METHOD

Dissipative particle dynamics is a mesoscale simulation, in which a group of atoms or molecules is coarse grained into a single DPD bead [27–31]. DPD simulation is essentially the same as molecular dynamics simulation, and the motion of DPD particles obeys Newton's equation of motion [27–31]. The forces acting on a DPD bead consist of three pairwise-additive, short-ranged interactions: conservative, dissipative, and random forces. The conservative force $\mathbf{F}^C$ is soft and repulsive, and the cutoff radius is r_c beyond which the interaction vanishes,

$$\mathbf{F}_{ij}^C = \begin{cases} a_{ij}(r_c - r_{ij})\hat{\mathbf{r}}_{ij}, & r_{ij} \leqslant r_c \\ 0, & r_{ij} > r_c \end{cases}. \quad (1)$$

Here $\hat{\mathbf{r}}_{ij}$ represents the unit vector joining beads i and j, and r_{ij} denotes the magnitude of the bead-bead vector. The interaction parameter a_{ij} describes the repulsion between beads i and j. Five types of DPD beads are used to represent lipid, copolymer, and water. For the same type of beads, $a_{ii} = 25$ is chosen to give the compressibility of the DPD fluid the same as water [32]. For different types of beads, a_{ij} deviates positively from 25 as their incompatibility is increased. The detailed descriptions of dissipative and random forces have been given elsewhere [31].

The initial structure of a hybrid membrane was constructed by randomly arranging lipids and copolymers with a specific ratio into a bilayer structure. The water beads were distributed outside the membrane. The modeled membrane was simulated in a cubic box under periodic boundary condition, and the total number of DPD beads was 98 304. The initial box size was 32 $\times$ 32 $\times$ 32, and relaxed via a barostat ($NP\gamma T$). The equation of motion was integrated by a velocity Verlet scheme. The time increment was $\Delta t = 0.01$. Surface tension of the membrane was obtained by $\gamma = \langle L_z[P_z - (P_x + P_y)/2]\rangle$, which depicted the ensemble average of the difference between the normal (P_z) and tangential pressure ($P_x + P_y$) multiplied by the height of the simulation box (L_z). By using the Langevin piston approach [33], the conditions of constant normal pressure and zero surface tension were maintained by adjusting the width and depth of the simulation box (L_x and L_y). Each simulation took at least 3×10^6 time steps to ensure a tensionless membrane [34]. All the units are nondimensionalized by the cutoff distance r_c, bead mass m, and temperature k_BT.

In this study, poly(ethylene oxide)-*b*-poly(propylene oxide) (PEO-*b*-PPO) is chosen as our modeled diblock copolymer. It is designated as A_3B_x, of which A and B beads represent approximately three hydrophilic PEO units and four hydrophobic PPO units, separately [35]. While the A block contains three beads, the B block is constructed by x beads, varying from 11 to 25 beads. Three types of phospholipids are considered, and designated as $H_3(T_6)_2$-NKN, where H and T denote the DPD beads for the hydrophilic head and hydrophobic tails, respectively. The lipid molecule consists of a head with three H beads and two tails with six T beads. The differences among those lipids are their number of kinks (N) in the tails, which correspond to saturated lipids (NK0) and unsaturated lipids (NK1 and NK2). Schematic diagrams of diblock copolymers and lipids are depicted in Figs. S1(a) and S1(b) in the Supplemental Material [36]. Adjacent beads in lipid and copolymer molecules are connected by virtual springs using a harmonic spring force, $\mathbf{F}_{ij}^S = -\sum_j k_s(r_{ij} - r_{eq})\hat{\mathbf{r}}_{ij}$. The spring constant is set as $k_s = 100$ and the equilibrium length is chosen as $r_{eq} = 0.4$ for lipids and $r_{eq} = 0.7$ for copolymers [25,31]. Furthermore, the bending force with the bending constant $k_\vartheta = 20$ is applied to the lipid tails to reinforce their stiffness. For saturated tails, the bond angle between two consecutive bonds is compelled to be close to the value of π. For unsaturated tails, another bending force is applied to mimic the double-bonded portions of the kink structure, which leads to the equilibrium bond angle of $2\pi/3$ [31].

The interaction parameter a_{ij} between two different species can be estimated from the Flory-Huggins χ_{ij} parameter by the relation, $a_{ij} = 25 + 3.497\chi_{ij}$ [32]. The incompatibility between the two species grows with the value of χ. In this work, the χ parameter between two species is obtained by their solubility parameters (δ) [33]. For example, the solubility parameters of a fatty acid (hydrophobic portion

TABLE I. The interaction parameter (a_{ij}) introduced in this article. A and B represent hydrophilic and hydrophobic segments of diblock copolymer. H and T denote hydrophilic head bead and hydrophobic tail bead of lipids. W is the water bead.

a_{ij}	W	A	B	H	T
W	25	30	50	26	75
A		25	70	28	55
B			25	45	26
H				25	50
T					25

of the lipid) and propylene oxide (hydrophobic portion of the copolymer) are $\delta \approx 9.1$ and $\approx 7.7\,\mathrm{cal}^{1/2}/\mathrm{cm}^{3/2}$. Their difference ($\Delta\delta = 1.4\,\mathrm{cal}^{1/2}/\mathrm{cm}^{3/2}$) yields the interaction parameter $a_{TB} \approx 26$ [37],which is close to $a_{ii} = 25$ associated with the same species. On the contrary, $\Delta\delta$ between hydrophilic and hydrophobic portions is quite large, leading to a_{ij} significantly greater than 25. The interaction parameters between different DPD beads are listed in Table I. In our system, the total volume fraction of water is kept a constant, 0.74. To obtain a specific composition of the hybrid membrane, the volume fractions of copolymers (φ_p) and lipids (φ_l) are changed accordingly. They are defined as

$$\varphi_p = \frac{\text{total number of polymer beads in the membrane}}{\text{total number of beads in the membrane}}, \tag{2}$$

$$\varphi_l = \frac{\text{total number of lipid beads in the membrane}}{\text{total number of beads in the membrane}}. \tag{3}$$

Note that $\varphi_p + \varphi_l = 1$.

The physical state of a hybrid membrane is closely associated with lipid fluidity. In order to characterize the fluidity of lipids, lateral lipid self-diffusivity (D_l) is calculated. D_l is a function of the lipid concentration (φ_l) and the hydrophobic block length of diblock copolymers (B_x). In this work, lipid diffusivity is acquired by employing the Green-Kubo relation, which relates the self-diffusivity to the velocity autocorrelation function [38]. On the x-y plane of a membrane, it is given by

$$D_l = \int_0^\infty \langle v_x(\tau) v_x(0)\rangle d\tau, \tag{4}$$

where $v_x(0)$ and $v_x(\tau)$ represent the velocities in the x direction of a lipid at time $= 0$ and τ, respectively. $\langle v_x(\tau)v_x(0)\rangle$ measures the correlation between the velocities of a lipid at different times along an equilibrium trajectory. In addition to the lateral lipid self-diffusivity, the influence of the thickness mismatch between lipids and copolymers on the lipid interdigitation is investigated as well. The extent of interdigitation between the bilayer leaflets can be calculated from the overlap in density profiles of the bilayer leaflets [39],

$$I_{LR} = \int_{-\infty}^{\infty} \frac{4\rho_L(z)4\rho_U(z)}{[\rho_L(z) + \rho_L(z)]^2} dz, \tag{5}$$

where the subscripts "L" and "U" denote the lower and upper bilayer leaflets, respectively.

III. RESULT AND DISCUSSION

In this work, the hybrid membrane is formed by the coassembly of $H_3(T_6)_2$ lipids and A_3B_x diblock copolymers with x varying from 11 to 25. Various factors which influence the mixing-demixing transition of hybrid membranes are explored, including the molar composition, cooling kinetics, lipid types, and energy incompatibility and thickness mismatch between lipids and copolymers. The fluidity of lipids in the two-component membrane is characterized by calculating lipid diffusivity. The dependence of lipid diffusivity on the state of the membrane and the B block length (x) is investigated as well.

A. Phase separation

After long-time evolution of the bilayer membrane containing the mixture of $H_3(T_6)_2$-NK0 lipids and A_3B_{11} diblock copolymers, the equilibrium structure is attained. Figure 1(a) shows the snapshots of the polymer-rich membrane assembled from various ratios of lipids and copolymers. When the amount of lipids is small, i.e., $\varphi_l \approx 5\%$, a homogeneous distribution of lipids in the membrane is observed. As φ_l exceeds a critical value ($\varphi_l^c \approx 10\%$), phase separation occurs, and there exist lipid-rich and polymer-rich phases. This result is consistent with experimental observations from giant unilamellar vesicles (GUVs) [16–18]. As demonstrated in the side view, both the upper and lower leaflets in the lipid-rich domain are occupied only by interdigitated lipids. From a thermodynamic point of view, this phase transition is the result of the competition between enthalpy and entropy contributions. In the regime of small φ_l, the entropy contribution dominates, and lipids tend to distribute uniformly in the membrane. As φ_l increases, the contribution of enthalpy grows due to the incompatibility between lipids and polymers. Eventually, phase separation appears in order to reduce the contact area between them.

In addition to the energy incompatibility between polymers and lipids, the effect of thickness mismatch has been reported as another key factor in the membrane structure [11,16–18]. The difference between the sizes of lipids and polymers can be realized from the thickness of the membrane containing lipids or polymers only. It is found that the membrane thickness of $H_3(T_6)_2$-NK0 lipids and A_3B_{11} polymers are comparable based on their hydrophobic layer thicknesses being 5.3 and 5.4, respectively. This consequence reveals that in such a hybrid membrane, the effect of thickness mismatch on the phase behavior may be insignificant. The phase change from a homogeneous distribution to two distinct domains with increasing φ_l is mainly driven by the unfavorable (van der Waals) interactions between lipids and polymers.

The transition from the homogeneous mixture of Dipalmitoylphosphatidylcholine (DPPC) lipids and PB-PEO polymers (mixing) to phase separation (demixing) has been experimentally observed by the thermally driven phase separation process [18]. The number and size of lipid-rich domains were tuned by controlling the cooling kinetics. Faster cooling rates result in the formation of smaller domains. In our work, the melting temperature of $H_3(T_6)_2$-NK0 lipids is $T_m \approx 1.05$, and the mixing phase is acquired for the membrane with $\varphi_l \approx 15\%$

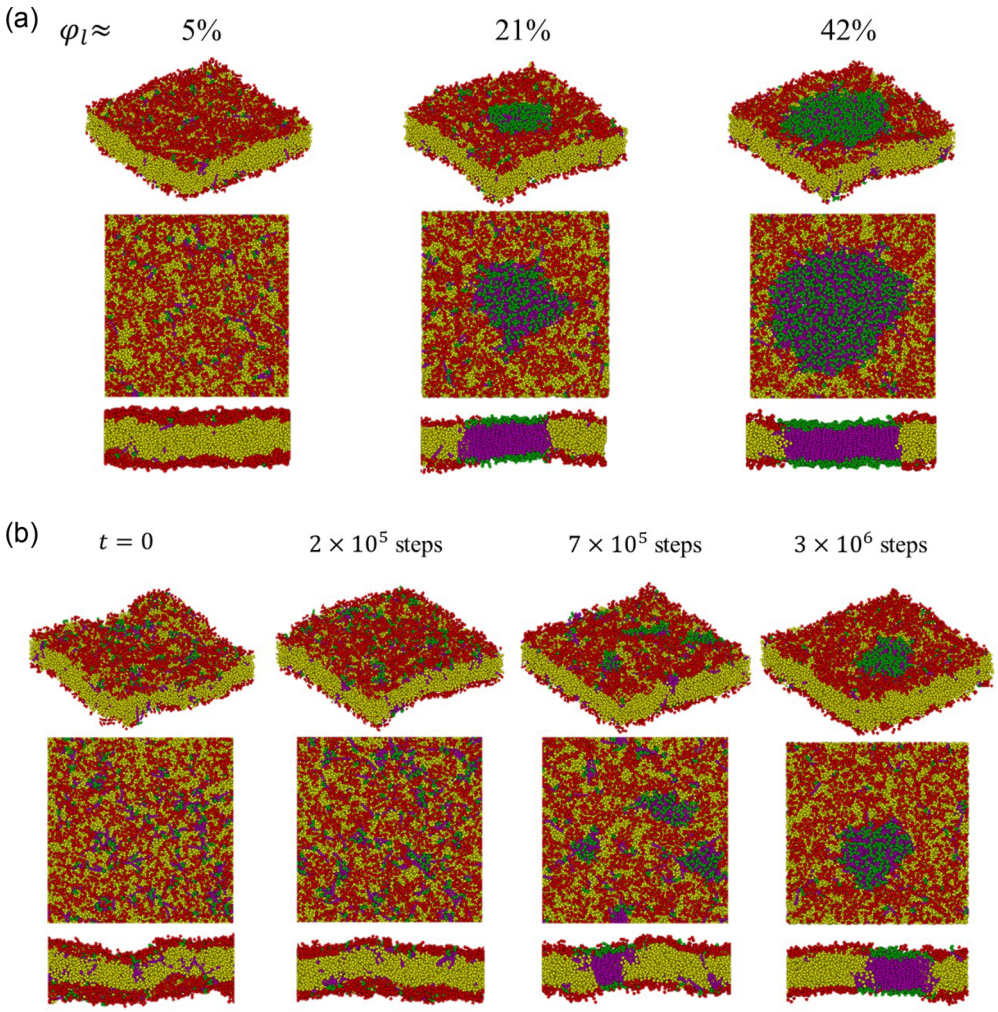

FIG. 1. (a) The snapshots of the polymer-rich membranes assembled from various ratios of $H_3(T_6)_2$-NK0 lipids and A_3B_{11} diblock copolymers. (b) The time evolution of a polymer-rich membrane assembled from $H_3(T_6)_2$-NK0 lipids and A_3B_{11} diblock copolymers with $\varphi_l \approx 15\%$.

as the system temperature is set as 1.3 ($T > T_m$) [31]. However, larger φ_l ($\sim$17%) still yields the demixing phase, revealing $\varphi_l^c(T = 1.3) > \varphi_l^c(T = 1.0)$. When T is lowered to 1.0 at $t = 0$, corresponding to a very fast quenching rate, the time evolution of the lipid-rich domains is shown in Fig. 1(b) for $\varphi_l \approx 15\%$. As time proceeds, several small-sized lipid-rich domains emerge. Gradually, those small domains come into contact by diffusion, and aggregate to form larger domains. Finally, a single lipid domain is found in the polymer-rich membrane. This result reveals that small-sized domains tend to cluster together to reduce the interfacial contacts between lipids and polymers. That is, the cooling rate can affect the formation kinetics of the lipid domains, but the development of a single lipid-rich domain is thermodynamically favorable.

When the lipid concentration exceeds 50%, the membrane becomes lipid rich, and phase separation persists. However, the polymer phase becomes a smaller domain surrounded by the lipid phase, as shown in Fig. 2(b) for polymer concentration $\varphi_p = 1 - \varphi_l \approx 15\%$. As the polymer concentration is low enough (i.e., $\varphi_p \approx 5\%$), polymers still tend to aggregate together in the upper or lower leaflet, as demonstrated in Fig. 2(a). However, the polymer cluster in the upper (lower) leaflet is in contact with only a few polymers in the lower (upper) leaflet. This feature of the polymer cluster in the lipid-rich membrane is distinct from that of the lipid cluster in the polymer-rich membrane. In the latter, the lipid cluster in one leaflet is always connected with approximately the same amount of lipids in the other leaflet. Note that a homogeneous distribution is seen for $\varphi_l \approx 5\%$ in the polymer-rich membrane. This result reveals that the incompatibility of a polymer in a lipid environment is stronger than that of a lipid in a polymer environment. In our simulation system, the hydrophobic tails of lipids are more rigid than the hydrophobic block of polymers because of the application of angle forces to the former. Lipids with two rigid tails may align in a more ordered manner than soft linear polymers. The incorporation of polymers into the lipid environment involves disruption of the more ordered lipid structure.

Although the polymer concentration ($\varphi_p \approx 5\%$) is low, the asymmetric structure of polymer clusters formed in the lipid bilayer leads to the deformation of the membrane. As a result, the planar membrane with zero surface tension fails to exist in the $NP\gamma T$ ensemble (evolving toward a giant aggregate eventually), and the significantly deformed membrane is

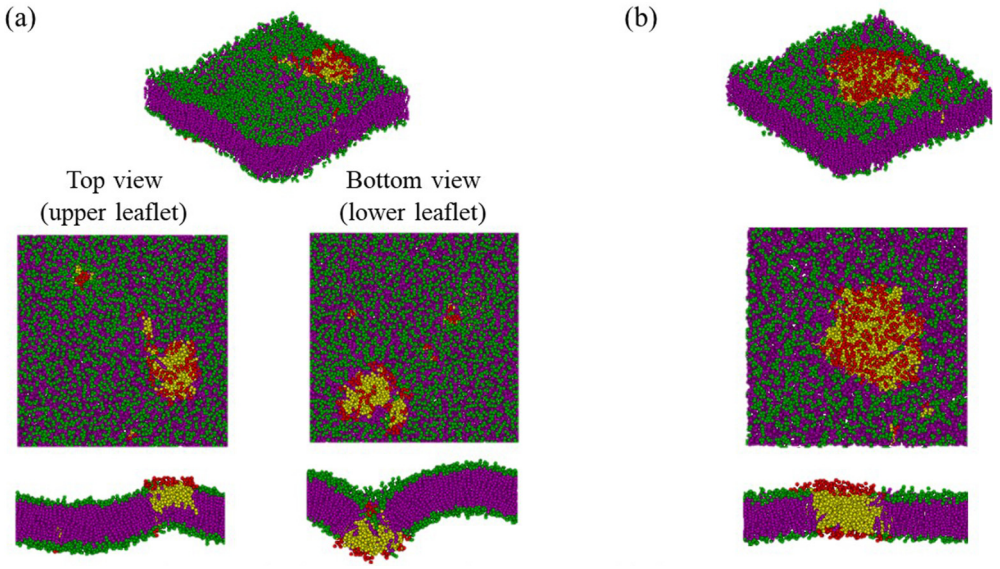

FIG. 2. The snapshots of the lipid-rich membranes assembled from two different ratios of $H_3(T_6)_2$ lipids and A_3B_{11} diblock copolymers at (a) $\varphi_p \approx 5\%$, and (b) $\varphi_p \approx 15\%$.

acquired by the *NVT* ensemble, as demonstrated in the side view of Fig. 2(a). Similar to the outcome of incorporation of an asymmetric nanoparticle in the membrane [40,41], the presence of an asymmetric cluster results in the deformation of the lipid bilayer in the immediate neighborhood of the cluster. That is, large spontaneous lipid curvature is induced by weak phase separation of polymers in a lipid-rich membrane, revealing that the formation of small hybrid vesicles is more favorable than giant ones. The mixing behavior and domain formation of giant hybrid vesicles of 1-palmitoyl-2-oleoylphosphatidylcholine (POPC) lipids and PB-b-PEO copolymers have been experimentally studied [17]. From confocal microscopy images, the polymer-rich GUVs can be intact for several weeks while the lipid-rich GUVs exhibit vesicle deformation significantly over time [17]. Evidently, the polymer-rich GUV is more stable than the lipid-rich GUV, consistent with our simulation results.

B. Critical lipid concentration and weak incompatibility between copolymer and lipids

The phase behavior of a hybrid membrane has been reported to change with lipids with different transition temperatures (T_m), which relate to lipid fluidity [11]. In this work, three kinds of lipids which have a different number of kinks in the lipid tails are considered. The transition temperature decreases with increasing the number of kinks (NK) [31]. At $T = 1.0$, the saturated lipid (NK $= 0$) is in the gel phase while kinked lipids (NK $= 1$ and 2) are in the fluid phase. In a polymer-rich membrane, the critical lipid concentration associated with the mixing-demixing transition was acquired from our simulations. Figure 3(a) shows the phase diagram of the hybrid membrane containing A_3B_{11} copolymers and $H_3(T_6)_2$ lipids with different NK. It depicts the physical state of the hybrid membrane (mixed or demixed state) as a function of the lipid concentration and the number of kinks. In the regimes of low and high lipid concentrations ($\varphi_l \langle 10\%$ and $\varphi_l \rangle 20\%$), all types of lipids (unkinked and kinked) behave the same: A single-phase membrane (mixing state) appears for small φ_l, while a lipid-rich domain (demixing state) is observed for high φ_l. Note that for saturated (unkinked) lipids at low φ_l, no phase separation is observed even at $T < T_m$ and for kinked lipids at high φ_l, phase separation occurs even at $T > T_m$. Obviously, lipid fluidity in a hybrid membrane cannot be determined solely by its transition temperature (T_m), and will be discussed later via lipid diffusivity. In the regime of the intermediate concentration ($10\% < \varphi_l < 20\%$), the hybrid membrane will undergo a phase transition from mixing to demixing as the lipid concentration exceeds a critical concentration ($\varphi_l > \varphi_l^c$), regardless of the lipid type. That is, there always exists φ_l^c, and it grows as the number of kinks increases.

As shown in Fig. 3(b), for saturated lipids (NK $= 0$) with $\varphi_l \approx 11\%$, a lipid-rich domain was formed because of $\varphi_l > \varphi_l^c$, as shown in the phase diagram at $T = 1.0$. However, when the system temperature rises to $T = 1.2$ ($T > T_m$), the mixing state takes place. This consequence indicates that φ_l^c is not only a function of the transition temperatures of pure lipids but also of the system temperature, $\varphi_l^c = f(T, T_m)$. In fact, we have performed simulations for saturated lipids (NK $= 0$) at different temperatures to find the corresponding critical lipid concentration. As shown in Fig. 4, φ_l^c is found to depend approximately linearly on T, and does not display a kinklike behavior around T_m. Because the entropy contribution ($-TS$) in the system free energy is proportional to the temperature, the increment of T favors the occurrence of the mixing state. As a result, it is anticipated that φ_l^c will grow with increasing the system temperature. Our simulation outcome agrees with this prediction. On the basis of the above arguments, one can conclude that the physical state (Φ) of a polymer-rich membrane can be simply determined by φ_l and φ_l^c; $\Phi = g(\varphi_l, \varphi_l^c)$. Because φ_l^c varies with T_m (lipid type) and T, one has $\Phi = g(\varphi_l, T, T_m)$. That is, the mixing-demixing transition in a hybrid membrane depends on the lipid concentration and system temperature, in addition to the lipid type. The

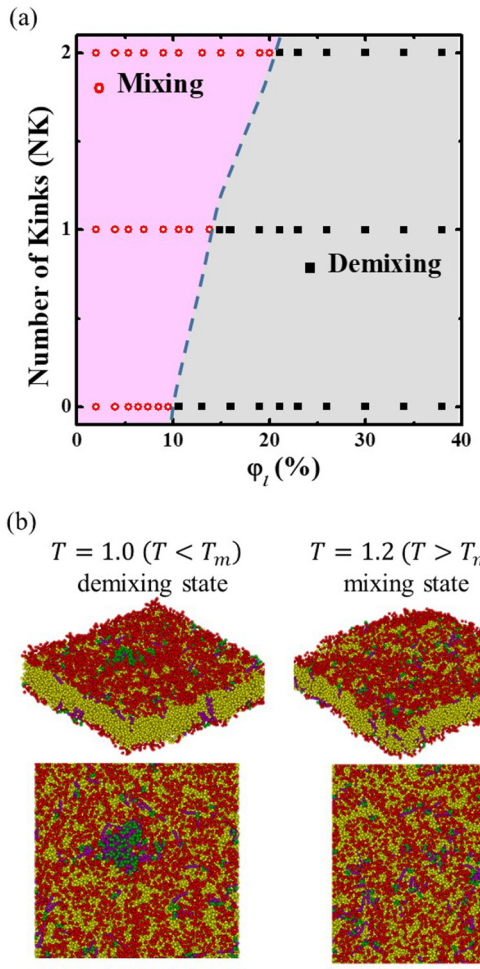

FIG. 3. (a) The phase diagram of a hybrid membrane containing $H_3(T_6)_2$ lipids and A_3B_{11} diblock copolymers. The equilibrium structure is a function of the number of kinks in the lipid tails and lipid concentration. (b) The demixing-mixing transition of unkinked lipids in a polymer-rich membrane with $\varphi_l \approx 11\%$ can be triggered by temperature.

above expression is only applicable to lipids with similar molecular architectures. If the molecular architectures of lipids are distinctly different, two lipids with the same T_m may give rise to different Φ at specified φ_l and T. Note that the effect of thickness mismatch for the hybrid membrane containing A_3B_{11} copolymers and $H_3(T_6)_2$ lipids is not significant.

To acquire a stable hybrid membrane, the prerequisite condition is believed to have weak incompatibility between lipids and copolymers [16,42]. In our simulation system, the energy incompatibility between two different species is decided by the Flory-Huggins χ parameter. For lipids and copolymers, the χ parameter between their hydrophilic portions is $\chi_{HA} \approx 0.86$ while that between their hydrophobic portions is $\chi_{TB} \approx 0.2$. Thus, one has $a_{HA} = 28$ and $a_{TB} = 26$. Those values of a_{ij} (close to 25) indicate that the energy incompatibility between lipids and copolymers is weak. In addition to the difference of their chemical constituents, there exists the structural incompatibility between two-tailed lipids and linear diblock copolymers. The packing structures of molecules generally depend on their molecular architectures. It is known that two-tailed lipids

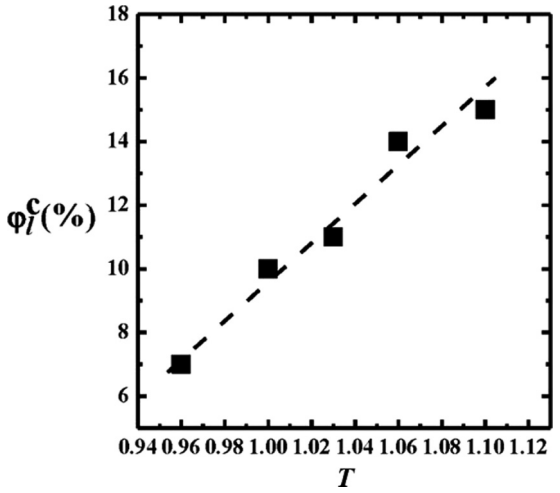

FIG. 4. φ_l^c (Critical lipid concentration) versus temperature (T) for saturated lipids (NK = 0).

prefer packing into lamellar structures while linear diblock copolymers tend to assemble into micelles or bilayers [43]. The role of the structural incompatibility for phase separation in a hybrid membrane is still unclear, and can be examined simply by simulations subject to the athermal condition.

The *athermal* hybrid membranes with various ratios of lipids and copolymers are achieved by setting $a_{HA} = 25$ and $a_{TB} = 25$. That is, the energy incompatibility in their hydrophilic layer (comprising H and A segments) or the hydrophobic layer (containing T and B segments) is turned off. A homogeneous distribution of lipids (mixing state) in the hybrid membrane is always observed for the athermal condition, even at high lipid concentrations, e.g., $\varphi_l \approx 42\%$. Note that phase separation of the hybrid membrane with weak incompatibility take places when $\varphi_l > 10\%$. For the lipid-rich membranes, the mixing state is also acquired for the athermal condition regardless of φ_p. These results reveal that in a hybrid membrane consisting of two-tailed lipids and linear diblock copolymers, the structural incompatibility between them is unable to drive phase separation. In other words, the driving force for demixing in a hybrid membrane is attributed to their energy incompatibility, even though it is weak.

The energy incompatibility has two origins: incompatibility in the hydrophilic layer and that in the hydrophobic layer. The influence of the two contributions on phase separation can be examined by turning off one of them. The incompatibility of the hydrophilic layer is demonstrated by turning off the incompatibility of the hydrophobic layer ($a_{HA} = 28$ and $a_{TB} = 26 \rightarrow 25$). As shown in Fig. 5(a) for $\varphi_l = 21\%$, a homogeneous distribution of lipids appears, indicating that the energy incompatibility in the hydrophilic layer is too weak to cause phase separation. On the contrary, turning off the incompatibility of the hydrophilic layer ($a_{HA} = 28 \rightarrow 25$ and $a_{TB} = 26$) fails to prevent phase separation, as demonstrated in Fig. 5(b). This consequence indicates that for the hybrid membrane containing lipids and diblock copolymers, the energy incompatibility between their hydrophobic segments is responsible for the occurrence of phase separation. To avoid phase separation, one has to choose the diblock copolymer with its hydrophobic block compatible to the lipid tail.

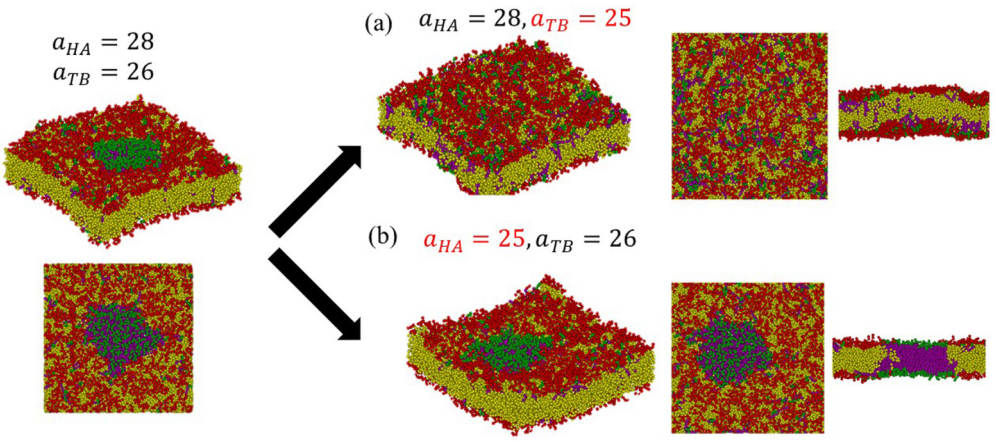

FIG. 5. (a) The snapshots of a polymer-rich membrane with $\varphi_l \approx 21\%$ when the energy incompatibility of the hydrophobic layer is turned off ($a_{HA} = 28,\ a_{TB} = 26 \rightarrow 25$). (b) The snapshots of a polymer-rich membrane with $\varphi_l \approx 21\%$ when the energy incompatibility of the hydrophilic layer is turned off ($a_{HA} = 28 \rightarrow 25,\ a_{TB} = 26$).

C. Lipid diffusivity and effect of thickness mismatch

Lipid fluidity is an important property associated with membrane functions. In a pure lipid membrane, lipid fluidity is generally dependent on the physical states of lipids (gel or liquid). However, in a hybrid (two-component) membrane, fluidity of lipids is not only affected by their physical state but also by their molar composition (φ_l). In order to explore the effects of φ_l, the diffusivity of lipids (D_l) in the hybrid membranes with different φ_l is calculated. As demonstrated in Fig. 6, D_l is plotted against φ_l for lipids containing the different number of kinks (NK). For a pure lipid membrane ($\varphi_l = 100\%$), it is known that the lipid possesses lower fluidity in its gel phase but exhibits higher fluidity in its fluid phase [44,45]. Our simulations show that the diffusivity of an unkinked lipid (in the gel phase) is significantly lower than that of kinked lipids (in the fluid phase) since in this work $T < T_m$ for an unkinked lipid but $T > T_m$ for kinked lipids. In addition, lipid diffusivity grows with increasing the number of kinks. The results are consistent with those reported in the literature [46]. Note that the point of abrupt change inferred from Fig. 6 differs from φ_l^c shown in Fig. 3 because of the significant boundary effect on D_l, which shall vanish in a macroscopic system.

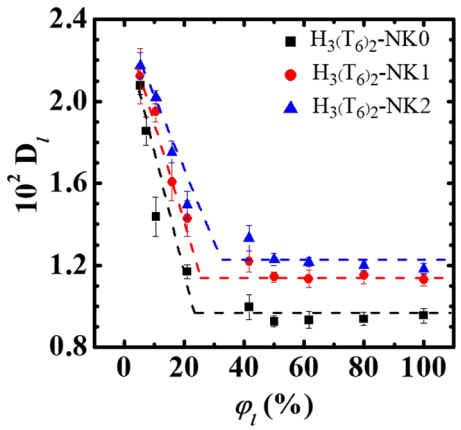

FIG. 6. The lateral diffusivity of lipids (D_l) is plotted against the lipid concentrations (φ_l) for different degrees of lipid unsaturation.

In a hybrid membrane, lipid diffusivity is highest when the lipid concentration approaches zero, as demonstrated in Fig. 6. For unkinked lipids, $D_l(\varphi_l = 5\%) \approx 2.07 \times 10^{-2}$ is approximately 2.2 times of that in the pure lipid membrane, $D_l(\varphi_l = 100\%) \approx 0.95 \times 10^{-2}$. Obviously, lipids move slower in the lipid-rich domain than in the polymer-rich domain. The former provides a more organized environment for lipids and hence hinders their random motion. As the lipid concentration is gradually increased, lipid diffusivity decreases quickly but reaches a constant value for large enough φ_l. The variation of lipid fluidity with the lipid concentration is qualitatively similar for all lipid types. Two regimes can be identified and they are closely related to phase transition. In the regime of low φ_l, lipids mix well with polymers and they can move fast in the polymer-surrounded environment. As φ_l is increased, the lipid-lipid contacts grow and hinder the lipid motion. In the regime of high enough φ_l, the lipid-rich domain appears and most lipids move in a way similar to that in a pure lipid membrane.

Up to now, only the hybrid membranes formed by A_3B_{11} diblock copolymers and $H_3(T_6)_2$ lipids have been studied because the thicknesses of their hydrophobic segments are comparable. Obviously, in the above situation thickness mismatch between them is not significant, and phase separation can occur due to energy incompatibility. In order to understand the influence of thickness mismatch on the phase behavior of the hybrid membrane, copolymers with different lengths of hydrophobic block (B_x) are considered. Figure 7(a) shows the snapshots of hybrid membranes containing diblock copolymers (A_3B_x) with x varying from 11 to 25 and unkinked lipids with $\varphi_l = 21.1\%$. As the hydrophobic length is increased, the lipid-rich domain is still observed for $x \leqslant 17$ but vanishes for $x \geqslant 21$, as illustrated in the top view of Fig. 7(a). In terms of interdigitation [Eq. (5)], positive values of interdigitation are obtained for $x \leqslant 17$, and it becomes zero for $x \geqslant 21$, as shown in Fig. 7(b). Obviously, the lipid concentration is high enough to develop the lipid-rich domain ($\varphi_l > \varphi_l^c$ for $x \leqslant 17$), and the effect of thickness mismatch is demonstrated in the vicinity of the lipid-polymer boundary, as shown in the side view of Fig. 7(a). To match the lipid and polymer domains (conformational adaption), the local membrane deformation

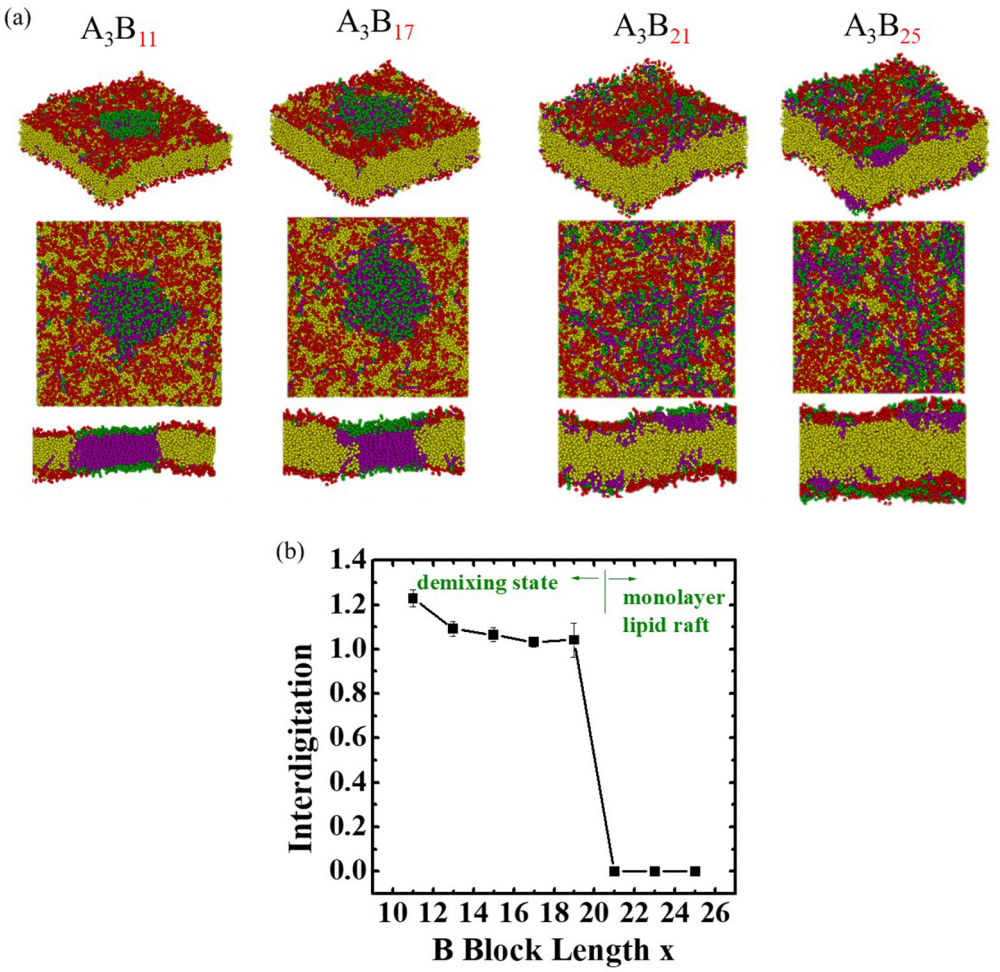

FIG. 7. (a) The snapshots of hybrid membranes containing diblock copolymers (A_3B_x) with x varying from 11 to 25 and unkinked lipids with $\varphi_l = 21.1\%$. (b) The extent of interdigitation of lipids is plotted against the B block length (x) at $\varphi_l = 21.1\%$ (the demixing state and monolayer lipid raft).

at the boundary becomes significant as x is increased. Furthermore, the decrease of interdigitation with increasing the hydrophobic length implies that the thickness of the lipid-rich domain is expanded by the polymer domain [see Fig. 7(b)]. However, the lipid-rich domain becomes unstable as the thickness mismatch is too large. As a result, the lipid-rich domain disintegrates, and several "lipid rafts" appear. The structure of lipid rafts (monolayer) is different from that of the lipid-rich domain (bilayer) associated with phase separation. The monolayer rafts float freely on either the upper or lower leaflet, and therefore no interdigitation is observed. Because of the asymmetric distribution of rafts on the two leaflets, the local spontaneous curvature of the membrane can be induced.

The influence of the hydrophobic block length of copolymers (B_x) on the phase behavior can be realized from lipid fluidity associated with thickness mismatch as well. Figure 8 shows the plot of lipid diffusivity (D_l) against the B block length (x) at $\varphi_l = 5.3\%$ (the mixing state) and $\varphi_l = 21.1\%$ (the demixing state and monolayer lipid raft). As long as lipids are homogeneously distributed in the hybrid membrane at $\varphi_l = 5.3\%$, D_l exhibits high mobility and is independent of x. That is, the lipid's motion encounters the same resistance from its environment, regardless of the membrane thickness. However, when the lipid-rich domain associated with the demixing state or monolayer lipid raft appears at $\varphi_l = 21.1\%$, D_l displays low mobility and varies with x. It is found that

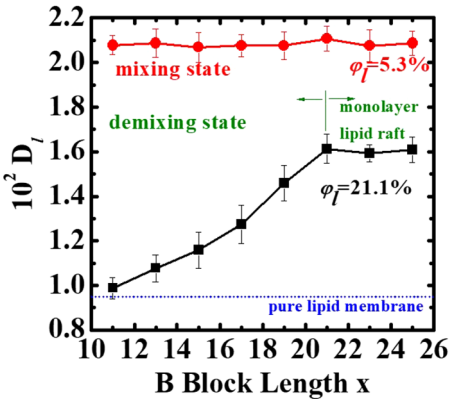

FIG. 8. Lateral lipid diffusivity (D_l) is plotted against B block length (x) at $\varphi_l = 5.3\%$ (the mixing state) and $\varphi_l = 21.1\%$ (the demixing state and monolayer lipid raft).

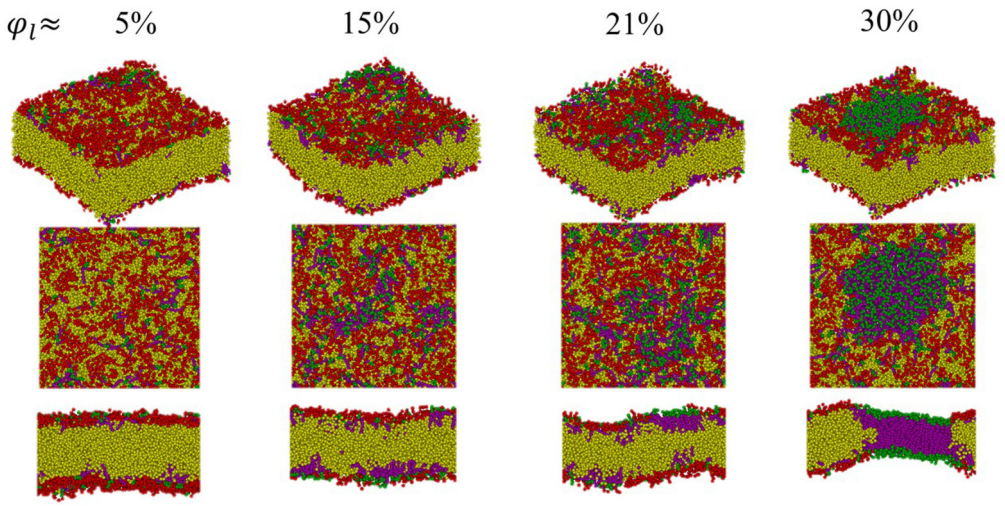

FIG. 9. The snapshots of the polymer-rich membranes assembled from various ratios of $H_3(T_6)_2$-NK0 lipids and A_3B_{21} diblock copolymers.

D_l grows with increasing x (from 11 to 19) but approaches a plateau ($x \geqslant 21$). In the ascending regime ($x \leqslant 19$), the lipid-rich domain with the bilayer structure corresponding to the demixing state prevails. As demonstrated in the side view of Fig. 7(a), the extent of lipid interdigitation is weakened with increasing x in order to reduce the effect of thickness mismatch, corresponding to conformation adaption. Since the resistance to the lipid motion in the bilayer due to lipid interdigitation is lowered, the lipid mobility rises with x. In the plateau regime ($x \geqslant 21$), monolayer lipid rafts with the monolayer structure dominate. Because lipid interdigitation vanishes, D_l is higher than those of interdigitated lipids and becomes insensitive to the membrane thickness. Compared to lipids surrounded by copolymers ($\varphi_l = 5.3\%$), D_l of lipids in the monolayer rafts has lower values due to frequent lipid-lipid contacts. Note that the extent of the variation of diffusivity from simulations is much less than that from experiments [45]. It has been attributed to the soft potential associated with the DPD beads, which leads to a fast diffusive transport close to their momentum transport. This may cause some difficulties to compare simulation results with real systems by the lipid diffusivity. Nonetheless, the qualitative behavior of diffusion remains correct.

The aforementioned results reveal that the demixing state lipid-rich domain with bilayer structures may disappear as the thickness mismatch effect becomes significant, although monolayer lipid rafts emerge. The question whether phase separation can still occur in the hybrid membrane with significant thickness mismatch arises naturally. To resolve this problem, the physical state of the hybrid membrane containing $H_3(T_6)_2$ lipids and A_3B_{21} diblock copolymers is examined for various molar compositions. Figure 9 shows the snapshots of the polymer-rich membrane with $\varphi_l \approx 5\%$–30%. At $\varphi_l \approx 15\%$, only a few monolayer lipid rafts are seen while phase separation (lipid-rich domain) takes place for A_3B_{11} copolymers [see Fig. 1(b)]. At $\varphi_l \approx 21\%$, the number of monolayer lipid rafts increases. However, at $\varphi_l \approx 30\%$, phase separation (bilayer structure) occurs eventually. This consequence reveals that the effect of thickness mismatch retards the occurrence of phase separation, and raises the critical lipid concentration (φ_l^c).

IV. CONCLUSION

A hybrid membrane consisting of A_3B_x diblock copolymers and $H_3(T_6)_2$-NKN lipids is investigated by DPD simulations. The hydrophobic block length varies from $x = 11$ to 25, and both saturated (NK0) and unsaturated (NK1, NK2) lipids are considered. When the effect of thickness mismatch is insignificant, the mixing-demixing transition in the polymer-rich membrane (A_3B_{11}) is always observed as the lipid concentration (φ_l) exceeds a critical value (φ_l^c). The critical lipid concentration varies with the lipid types and depends on the main transition temperature of lipids (T_m) and system temperature. Phase separation is driven by weak energy incompatibility between lipids and copolymers. The demixing state vanishes as the athermal condition in the hydrophobic layer is satisfied.

In addition to φ_l and T_m, the physical state of a hybrid membrane is also influenced by thickness mismatch. In the crossover from the mixing to demixing state, the state of monolayer lipid rafts emerges as thickness mismatch becomes significant. That is, the occurrence of the lipid-rich domain with the bilayer structure is retarded by thickness mismatch in the A_3B_{21} membrane. Lipid diffusivity (D_l) characterizing lipid fluidity depends significantly on the state of the hybrid membrane, besides T_m. Compared to lipid-polymer interactions, the resistance to the lipid motion comes mainly from lipid-lipid interactions and interdigitations. As a result, lipids exhibit higher mobility in the mixing state, and display lower mobility in the demixing state. As the hydrophobic B block length (x) is increased, the lipid-rich domain becomes less interdigitated. Therefore, D_l grows with increasing x for $x =$ 11–19 in the demixing state. For thick membranes ($x \geqslant 21$), D_l approaches a plateau due to the absence of interdigitation for monolayer lipid rafts.

ACKNOWLEDGMENTS

This research work is supported by Ministry of Science and Technology, Taiwan. Computing times provided by the National Taiwan University Computer and Information Networking Center are gratefully acknowledged.

[1] J. Grumelard, A. Taubert, and P. Meier, Soft nanotubes from amphiphilic ABA triblock macromonomers, Chem. Commun. **0**, 1462 (2004).

[2] L. Zhang and A. Eisenberg, Multiple morphologies of crew-cut aggregates of polystyrene-*b*-poly(acrylic acid) block copolymers, Science **268**, 1728 (1995).

[3] C. Draghici, J. Kowal, A. Darjan, W. Meier, and C. G. Palivan, Active surfaces formed by immobilization of enzymes on solid-supported polymer membranes, Langmuir **30**, 11660 (2014).

[4] J. Ł. Kowal, J. K. Kowal, D. Wu, H. Stahlberg, C. G. Palivan, and W. P. Meier, Functional surface engineering by nucleotide-modulated potassium channel insertion into polymer membranes attached to solid supports, Biomaterials **35**, 7286 (2014).

[5] J. P. Colletier, B. Chaize, M. Winterhalter, and D. Fournier, Protein encapsulation in liposomes: efficiency depends on interactions between protein and phospholipid bilayer, BMC Biotechnol. **2**, 9 (2002).

[6] J. O. Eloy, M. C. de Souza, R. Petrilli, J. P. A. Barcellos, R. J. Lee, and J. M. Marchetti, Liposomes as carriers of hydrophilic small molecule drugs: strategies to enhance encapsulation and delivery, Colloids Surf., B **123**, 345 (2014).

[7] A. D. Ostrowski, B. F. Lin, M. V. Tirrell, and P. C. Ford, Liposome encapsulation of a photochemical NO precursor for controlled nitric oxide release and simultaneous fluorescence imaging, Mol. Pharmaceutics **9**, 2950 (2012).

[8] E. Blanco, H. Shen, and M. Ferrari, Principles of nanoparticle design for overcoming biological barriers to drug delivery, Nat. Biotechnol. **33**, 941 (2015).

[9] M. Kanamala, W. R. Wilson, M. Yang, B. D. Palmer, and Z. Wu, Mechanisms and biomaterials in pH-responsive tumour targeted drug delivery: A review, Biomaterials **85**, 152 (2016).

[10] V. P. Torchilin, Multifunctional, stimuli-sensitive nanoparticulate systems for drug delivery, Nat. Rev. Drug Discovery **13**, 813 (2014).

[11] M. Chemin, P.-M. Brun, S. Lecommandoux, O. Sandre, and J.-F. Le Meins, Hybrid polymer/lipid vesicles: fine control of the lipid and polymer distribution in the binary membrane, Soft Matter **8**, 2867 (2012).

[12] T. Azzam and A. Eisenberg, Control of vesicular morphologies through hydrophobic block length, Angew. Chem., Int. Ed. **45**, 7443 (2006).

[13] G. P. Robbins, R. L. Saunders, J. B. Haun, J. Rawson, M. J. Therien, and D. A. Hammer, Tunable leuko-polymersomes that adhere specifically to inflammatory markers, Langmuir **26**, 14089 (2010).

[14] R. R. García, M. Mell, I. L. Montero, J. Netzel, T. Hellweg, and F. Monroy, Polymersomes: smart vesicles of tunable rigidity and permeability, Soft Matter **7**, 1532 (2011).

[15] J. S. Lee and J. Feijen, Polymersomes for drug delivery: design, formation and characterization, J. Controlled Release **161**, 473 (2012).

[16] J.-F. Le Meins, C. Schatz, S. Lecommandoux, and O. Sandre, Hybrid polymer/lipid vesicles: state of the art and future perspectives, Mater. Today **16**, 397 (2013).

[17] J. Nam, P. A. Beales, and T. K. Vanderlick, Giant phospholipid/block copolymer hybrid vesicles: mixing behavior and domain formation, Langmuir **27**, 1 (2011).

[18] J. Nam, T. K. Vanderlick, and P. A. Beales, Formation and dissolution of phospholipid domains with varying textures in hybrid lipo-polymersomes, Soft Matter **8**, 7982 (2012).

[19] F. A. Heberle, R. S. Petruzielo, J. Pan, P. Drazba, N. Kučerka, R. F. Standaert, G. W. Feigenson, and J. Katsaras, Bilayer thickness mismatch controls domain size in model membranes, J. Am. Chem. Soc. **135**, 6853 (2013).

[20] M. Xiao, J. Liu, J. Yang, R. Wang, and D. Xie, Biomimetic membrane control of block copolymer vesicles with tunable wall thickness, Soft Matter **9**, 2434 (2013).

[21] M. Schulz and W. H. Binder, Mixed hybrid lipid/polymer vesicles as a novel membrane platform, Macromol. Rapid Commun. **36**, 2031 (2015).

[22] T. M. Kuo and H. W. Gardner, *Lipid Biotechnology* (Macrcel Dekker, New York, 2002).

[23] M. Roth, Solubility parameter of poly(dimethyl siloxane) as a function of temperature and chain length, J. Polym. Sci., Part B: Polym. Phys. **28**, 2715 (1990).

[24] J. Brandrup, E. H. Immergut, and E. A. Grulke, *Polymer Handbook*, 4th ed. (John Wiley & Sons, New York, 2005).

[25] Y. L. Yang, M. Y. Chen, H.-K. Tsao, and Y.-J. Sheng, Dynamics of bridge-loop transformation in a membrane with mixed monolayer/bilayer structures, Phys. Chem. Chem. Phys. **20**, 6582 (2018).

[26] A. F. Jakobsen, Constant-pressure and constant-surface tension simulations in dissipative particle dynamics, J. Chem. Phys. **122**, 124901 (2005).

[27] P. J. Hoogerbrugge and J. M. V. A. Koelman, Simulating microscopic hydrodynamic phenomena with dissipative particle dynamics, Europhys. Lett. **19**, 155 (1992).

[28] Y.-F. Chen, S. Xiao, H.-Y. Chen, Y.-J. Sheng, and H.-K. Tsao, Enhancing rectification of a nano-swimmer system by multi-layered asymmetric barriers, Nanoscale **7**, 16451 (2015).

[29] C.-Y. Teng, Y.-J. Sheng, and H.-K. Tsao, Boundary-induced segregation in nanoscale thin films of athermal polymer blends, Soft Matter **12**, 4603 (2016).

[30] C.-Y. Teng, Y.-J. Sheng, and H.-K. Tsao, Surface segregation and bulk aggregation in an athermal thin film of polymer–nanoparticle blends: strategies of controlling phase behavior, Langmuir **33**, 2639 (2017).

[31] H.-L. Wu, Y.-J. Sheng, and H.-K. Tsao, Dynamic and mechanical properties of supported lipid bilayers, J. Chem. Phys. **144**, 154904 (2016).

[32] R. D. Groot and P. B. Warren, Dissipative particle dynamics: bridging the gap between atomistic and mesoscopic simulation, J. Chem. Phys. **107**, 4423 (1997).

[33] S. E. Feller, Y. Zhang, and R. W. Pastor, Constant pressure molecular dynamics simulation: the Langevin piston method, J. Chem. Phys. **103**, 4613 (1995).

[34] D. Morozova, M. Weiss, and G. Guigas, Shape as a determinant of membrane protein cluster formation, Soft Matter **8**, 11905 (2012).

[35] A. De Nicola, S. Hezaveh, Y. Zhao, T. Kawakatsu, D. Roccatano, and G. Milano, Micellar drug nanocarriers and biomembranes: how do they interact, Phys. Chem. Chem. Phys. **16**, 5093 (2014).

[36] See Supplemental Material at http://link.aps.org/supplemental/10.1103/PhysRevE.99.012403 for schematic diagrams of the mappings between realistic lipids and model lipids.

[37] A. F. M. Barton, *Handbook of Polymer-Liquid Interaction Parameters and Solubility Parameters* (CRC Press, Boca Raton, FL, 1990).

[38] D. Frenkel and B. Smit, *Understanding Molecular Simulation* (Academic Press, New York, 2001).

[39] R. Hartkamp, T. C. Moore, C. R. Iacovella, A. T. Michael, P. A. Bulsara, D. J. Moore, and C. McCabe, J. Phys. Chem. B **120**, 12863 (2016).

[40] A. M. Kabbani and C. V. Kelly, The detection of nanoscale membrane bending with polarized localization microscopy, Biophys. J. **113**, 1782 (2017).

[41] B. Różycki and R. Lipowsky, Spontaneous curvature of bilayer membranes from molecular simulations: Asymmetric lipid densities and asymmetric adsorption, J. Chem. Phys. **142**, 054101 (2015).

[42] T. P. T. Dao, F. Fernandes, E. Ibarboure, K. Ferji, M. Prieto, O. Sandre, and J. F. Le Meins, Modulation of phase separation at the micron scale and nanoscale in giant polymer/lipid hybrid unilamellar vesicles (GHUVs), Soft Matter **13**, 627 (2017).

[43] D. D. Lasic, *Liposomes: From Physics to Applications* (Elsevier Science Ltd, Amsterdam, 1993).

[44] G. M'Baye, Y. Mély, G. Duportail, and A. S. Klymchenko, Liquid ordered and gel phases of lipid bilayers: fluorescent probes reveal close fluidity but different hydration, Biophys. J. **95**, 1217 (2008).

[45] D. A. Los and N. Murata, Membrane fluidity and its roles in the perception of environmental signals, Biochim. Biophys. Acta **1666**, 142 (2004).

[46] S. J. Marrink, J. Risselada, and A. E. Mark, Simulation of gel phase formation and melting in lipid bilayers using a coarse grained model, Chem. Phys. Lipids. **135**, 223 (2005).